Halogen-Dependent Surface Confinement Governs Selective Alkane Functionalization to Olefins

*Guido Zichittella[+], Matthias Scharfe[+], Begoña Puértolas, Vladimir Paunović, Patrick Hemberger, Andras Bodi, László Szentmiklósi, Núria López, and Javier Pérez-Ramírez**

Abstract: *The product distribution in direct alkane functionalization by oxyhalogenation strongly depends on the halogen of choice. We demonstrate that the superior selectivity to olefins over an iron phosphate catalyst in oxychlorination is the consequence of a surface-confined reaction. By contrast, in oxybromination alkane activation follows a gas-phase radical-chain mechanism and yields a mixture of alkyl bromide, cracking, and combustion products. Surface-coverage analysis of the catalyst and identification of gas-phase radicals in operando mode are correlated to the catalytic performance by a multi-technique approach, which combines kinetic studies with advanced characterization techniques such as prompt-gamma activation analysis and photoelectron photoion coincidence spectroscopy. Rationalization of gas-phase and surface contributions by density functional theory reveals that the molecular level effects of chlorine are pivotal in determining the stark selectivity differences. These results provide strategies for unraveling detailed mechanisms within complex reaction networks.*

The development of novel technologies for the selective functionalization of light alkanes is a critical step to enable the utilization of natural gas as an energy vector in the transition between the oil and the renewables era.[1] This pivotal advancement is limited by our understanding of the mechanisms governing the heterogeneously catalyzed reactions for direct hydrocarbon upgrading, which can provide design criteria for active, selective, and stable catalysts. In the case of light-alkane functionalization—generally requiring high temperatures and/or aggressive reactants—the level of complexity is further amplified by the possibility of gas-phase reaction pathways, in which highly reactive radical species and/or radical initiators are liberated from the surface to generate desired and undesired products.[2] A high level of selectivity control could be achieved if alkane activation were confined on a catalyst surface. However, to unravel reaction pathways, as well as reactive intermediates in gaseous and solid phases, and to model complex and dynamic surfaces at the atomic level, the combined use of strong experimental evidence with advanced theoretical approaches is required. Catalytic oxychlorination, which involves the reaction of an alkane with HCl and O_2, has recently demonstrated selective ($\geq 95\,\%$) generation of ethylene from ethane over a wide range of catalyst families,[3] while the use of HBr as a halide source results in a range of products comprising alkyl bromide, CH_4, and carbon oxides, among others.[4] To understand the mechanistic origin of such selectivity control, we combined kinetic studies with operando surface-coverage quantification by prompt-gamma activation analysis (PGAA) and monitoring of gas-phase radicals by photoelectron photoion coincidence spectroscopy (PEPICO), ultimately rationalized at the molecular level by density functional theory (DFT) calculations (Figure 1). An iron phosphate catalyst was chosen because of its ability to selectively ($\leq 97\,\%$) generate ethylene and propylene via alkane oxychlorination.[3] Performance assessments in ethane oxychlorination (EOC) and oxybromination (EOB), under variable temperatures (573–853 K), revealed that the light-off curve for oxybromination was shifted to about 150 K—a lower temperature compared to that obtained in oxychlorination (Figure 2a) and in agreement with previous observations on other materials.[4b] Characterization of the material before and after catalysis by means of N_2 sorption, X-ray diffraction (XRD), and Raman spectroscopy revealed that the textural properties and the crystallographic structure were preserved (Supporting Information, Figure S1, Table S2). A comparison of the selectivity patterns obtained at a similar alkane conversion level (ca. 20 %) showed that C_2H_4 is the major product (selectivity ca. 95 %) when HCl is used as a halide source, while oxybromination led to the formation of C_2H_5Br, CH_4, carbon oxides, and C_2H_4 (Figure 2b; Figure S2). Both reactions are believed to follow a consecutive mechanism, where the alkyl halide is the intermediate to the olefin (Figure S2). Nevertheless, the observed selectivity differences might be caused by the

[*] G. Zichittella,[+] M. Scharfe,[+] Dr. B. Puértolas, Dr. V. Paunović, Prof. J. Pérez-Ramírez
Institute for Chemical and Bioengineering, Department of Chemistry and Applied Biosciences, ETH Zurich
Vladimir-Prelog-Weg 1, 8093 Zurich (Switzerland)
E-mail: jpr@chem.ethz.ch

Dr. P. Hemberger, Dr. A. Bodi
Laboratory of Femtochemistry and Synchrotron Radiation
Paul Scherrer Institute
5232 Villigen (Switzerland)

Dr. L. Szentmiklósi
Nuclear Analysis and Radiography Department, Centre for Energy Research, Hungarian Academy of Sciences
Konkoly-Thege Miklósi út 29–33, 1121 Budapest (Hungary)

Prof. N. López
Institute of Chemical Research of Catalonia
The Barcelona Institute of Science and Technology
Av. Països Catalans 16, 43007 Tarragona (Spain)

[+] These authors contributed equally to this work.

Supporting information, including catalyst preparation, characterization, and evaluation, descriptions of the operando PGAA and PEPICO techniques, DFT calculations, and the ORCID identification number(s) for the author(s) of this article can be found under: https://doi.org/10.1002/anie.201811669.

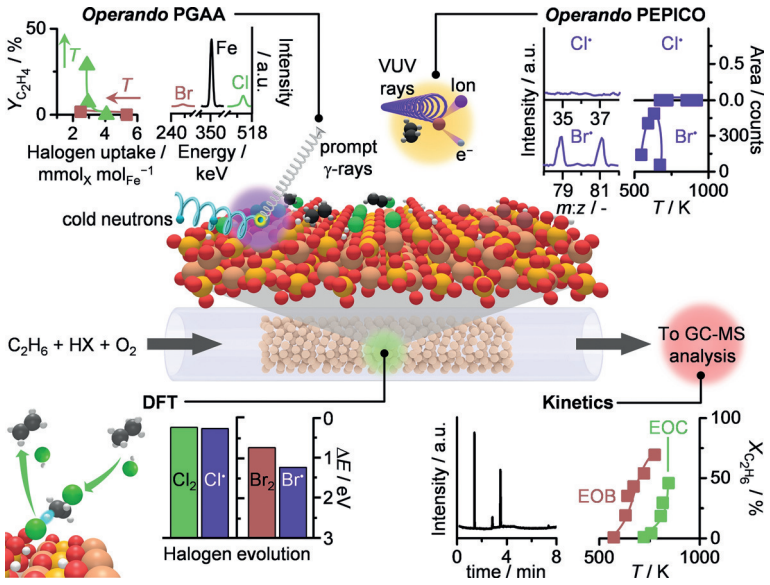

Figure 1. A representation of the multi-technique strategy used in this study that enabled unraveling of the surface-driven and gas-phase radical-chain pathways through which alkane activation occurs in catalytic ethane oxyhalogenation. This approach concertedly combined 1) kinetic analysis for assessment of catalytic activity and selectivity patterns with operando 2) PGAA and 3) PEPICO spectroscopies, enabling quantification of the surface composition and detection of gaseous intermediates, respectively. The experimental findings were ultimately rationalized by 4) DFT calculations. Each of these techniques results in spectra, or energy levels (inner graphs), that can be subsequently evaluated and/or correlated to observable parameters (outer graphs), revealing a detailed mechanistic picture for a complex chemical process.

more kinetically favorable elimination of HCl compared to HBr over a catalyst surface, as shown in catalytic methyl halide coupling.[5] To probe this hypothesis, we conducted ethyl halide dehydrohalogenation to C_2H_4 over $FePO_4$ (Figure S3) and observed that the light-off curve for C_2H_5Cl dehydrochlorination was shifted by about 40 K, to lower temperature, compared to C_2H_5Br. When O_2 and HX were co-fed with ethyl halide over $FePO_4$ (Figure 2c), dehydrochlorination led mainly to C_2H_4, while a competition between polybromination and dehydrobromination was evident for ethyl bromide. Additionally, catalytic hydrogen halide oxidation and gas-phase ethane halogenation were investigated so as to measure the ability of the catalyst to produce molecular halogen and the intrinsic reactivity of the halogen with the alkane at comparable conditions to oxyhalogenation (Figure 2a; Figure S4). While chlorine-based reactions occurred in distinct temperature regions, the bromine-based analogues overlapped, which indicates that adsorbed HCl cannot evolve as Cl_2 from the catalyst under typical oxychlorination conditions, in contrast to Br_2 that can be generated during oxybromination. These findings suggest that ethane oxychlorination could occur via a surface-driven mechanism in which the adsorbed chlorine species might be important for the catalyst performance. On the contrary, gas-phase bromination with in-situ-generated bromine species is likely the preferred pathway for ethane activation in oxybromination.

To address the impact of the halogen coverage on the performance, we conducted PGAA spectroscopy under operando conditions (for the principle of PGAA see Scheme S1), for which $FePO_4$ is a suitable material because of its moderate neutron-capture cross-section.[6] The experimental setup comprises a continuous-flow tubular reactor, where the catalyst is non-destructively irradiated with cold neutrons[7] that are captured by the nuclei of all atoms in the sampling volume during the oxyhalogenation reaction. The de-excitation of the thus formed compound nuclei results in emission of prompt γ-rays with element-specific energies and with intensities that are proportional to the number of emitting atoms (Figure 1). The quantified halogen uptake with respect to iron, and at variable temperatures and inlet HX concentrations, is correlated with the yield of ethylene in Figure 3. In particular, at the onset of oxychlorination, $FePO_4$ exhibited approximately 4.1 $mmol_{Cl}\,mol_{Fe}^{-1}$ chlorine uptake, which corresponds to 76% of surface iron sites occupied by chlorine. A rise in reaction temperature led to an increase of the yield of ethylene while the chlorine uptake decreased to approximately 3 $mmol_{Cl}\,mol_{Fe}^{-1}$ (equivalent to 55% surface coverage) and remained constant at higher temperatures. On the other hand, the bromine uptake at the onset of oxybromination at 573 K reached full coverage at approximately 5.4 $mmol_{Br}\,mol_{Fe}^{-1}$, which drastically decreased to 2.5 $mmol_{Br}\,mol_{Fe}^{-1}$ at 633 K. Further increase in temperature to 723 K did not allow bromine uptake quantification because of statistically negligible halogen content, as corroborated by the absence of bromine in the used catalyst by elemental analysis (Table S2). Interestingly, an increment of the halide feed resulted in an increased olefin yield that correlated with a higher halogen coverage in oxychlorination, while the opposite trend was observed in oxybromination. To translate these observations into causality correlations, density functional theory calculations were performed on the experimentally relevant (102) surface of trigonal $FePO_4$ (Figure S1). Cl_2 and Cl$^\bullet$ desorption are endothermic by 2.70 eV and 2.66 eV, respectively, indicating that chlorine atoms are persistent on the surface. In contrast, bromine can desorb as Br_2 ($\Delta E = 2.10$ eV), and even more favorably as Br$^\bullet$ ($\Delta E = 1.52$ eV, Figure 5; Figure S5). Therefore, the evolution of bromine species is much more energetically favored compared to chlorine species, which explains the lower surface bromination under comparable reaction conditions (Figures 2a and 3; Figure S5). These results suggest that gas-phase pathways can be initiated by the formation of bromine radicals, which were evidenced by the detection of Br_2, Br$^\bullet$, and $C_2H_5^\bullet$ radicals by operando PEPICO (Figure 4; Figures S6–S11). This spectroscopic technique, whose principle is schematized in Scheme S2, has recently revealed evidence of the gas-phase radical-chain routes in methane oxybromination.[2e] Therein, the gaseous species exiting the PEPICO reactor form a molecular beam that is skimmed and ionized by monochromatic vacuum ultraviolet (VUV) radiation to yield photoelectrons and photoions that are detected in

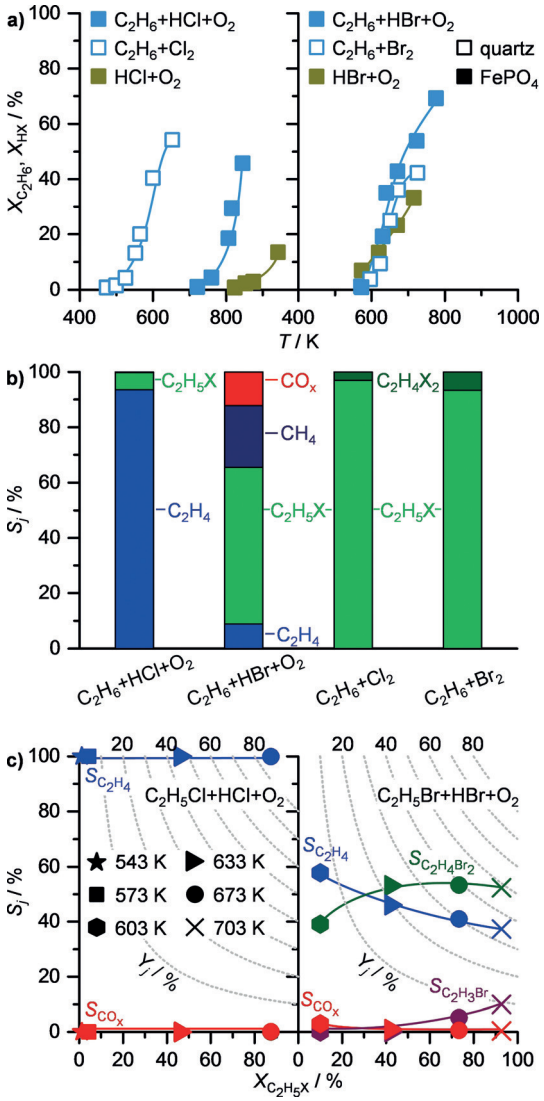

Figure 2. a) Ethane conversion as a function of temperature in oxyhalogenation over $FePO_4$ and in non-catalytic ethane halogenation over inert quartz particles, and hydrogen halide conversion as a function of temperature in HX (X = Cl, Br) oxidation over $FePO_4$. These reactions occur in distinct temperature regions where chlorine chemistry is concerned, whereas they overlap for bromine chemistry. b) Selectivity patterns obtained in catalytic ethane oxyhalogenation and non-catalytic ethane halogenation at ca. 20% ethane conversion, illustrating that only ethane oxychlorination leads to selective ethylene generation. c) Selectivity to products as a function of ethyl halide conversion in the dehydrohalogenation of ethyl halide in the presence of HX and O_2 over $FePO_4$, showing that ethylene generation is favored with an ethyl chloride intermediate over its brominated counterpart. The dotted gray lines denote the yield of product *j* and the different symbols refer to the reaction temperature. Conditions in (a) and (b): C_2H_6:HX(X_2):O_2:Ar:He = 6:6(3):3(0):4.5:80.5(86.5), F_T = 100 cm^3 min^{-1}, W_{cat} = 1 g, P = 1 bar. Conditions in (c): C_2H_5X:HX:O_2:Ar:He = F1:6:3:4.5:85.5, F_T = 100 cm^3 min^{-1}, W_{cat} = 1 g, P = 1 bar.

delayed coincidence. In this way, isomer-selective identification of reactants and products is permitted, including radical intermediates in both ethane oxychlorination and oxybromination (Figures 1 and 4; Figures S6–S11).[8] In particular, the evolution of signals corresponding to reaction intermediates,

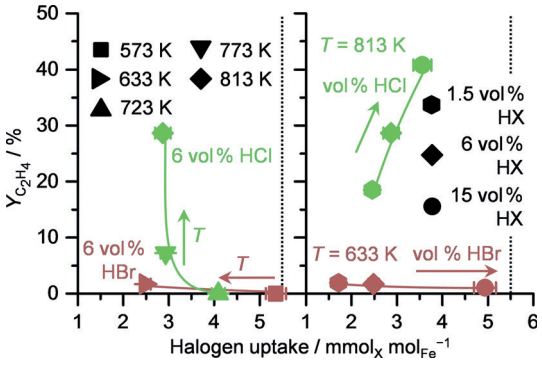

Figure 3. Yield of ethylene as a function of halogen uptake in ethane oxyhalogenation at different temperatures and HX (X = Cl, Br) inlet concentration as determined in operando PGAA. More details on the working principles of this technique are summarized in Scheme S1. Conditions: C_2H_6:HX:O_2:Ar:He = 6:6:3:4.5:80.5, F_T = 100 cm^3 min^{-1}, W_{cat} = 1 g, P = 1 bar. Dotted lines represent the calculated halogen uptake corresponding to full surface coverage. Error bars are presented for each catalytic point of the measured halogen uptake.

as a function of temperature, was correlated with that of the reaction products; while the Br_2 signal decreased sharply, signals associated with $C_2H_5^{\bullet}$ and Br$^{\bullet}$ radicals increased along with C_2H_5Br, until 600 K. At higher temperatures, the signal corresponding to C_2H_5Br dropped to zero, while that of the radicals and C_2H_4 increased, which is consistent with a higher rate of dehydrobromination compared to ethyl bromide generation (Figure 4; Figure S8). On the other hand, neither Cl_2 nor Cl$^{\bullet}$ radicals were observed under oxychlorination conditions in the investigated temperature range (Figure 4; Figure S6), which is in line with the DFT results. Furthermore, C_2H_5Cl decreased sharply with temperature while C_2H_4 increased, corroborating the occurrence of a consecutive mechanism in which ethane is transformed into ethyl halide that is consequently dehydrohalogenated to C_2H_4, as supported by steady-state experiments (Figure S2). Finally, measurements conducted using an empty reactor showed no production of radicals or products (Figures S10 and S11).

Computational investigations at the molecular level revealed that all the elementary steps in the gas-phase pathways of oxybromination were barrierless. Additionally, ethane or ethyl bromide activation with a Br$^{\bullet}$ radical, to form HBr, is endothermic by only 0.5 eV, while recombination of the produced radicals with Br$^{\bullet}$ to form C_2H_5Br or $C_2H_4Br_2$, which is occurring with a comparable collision frequency as activation, is strongly exothermic (> 2.5 eV, Figure S13). This implies that, once a bromine radical evolves from the surface, it will directly activate ethane or ethyl bromide, or consume any hydrocarbon radicals by recombination, thereby allowing inordinate polybromination instead of ethylene generation. Additionally, this mechanism of ethane activation can explain the apparent lower activation energy for ethane conversion in oxybromination (Figure 2a), which consistently opposes the DFT results for surface-catalyzed alkane activation in this reaction (Figure S14). Nonetheless, $C_2H_5^{\bullet}$ radicals were observed by operando PEPICO in oxychlorination as well, and its signal increased with the reaction temperature (Figure 4). Its occurrence in oxychlorination, in which the

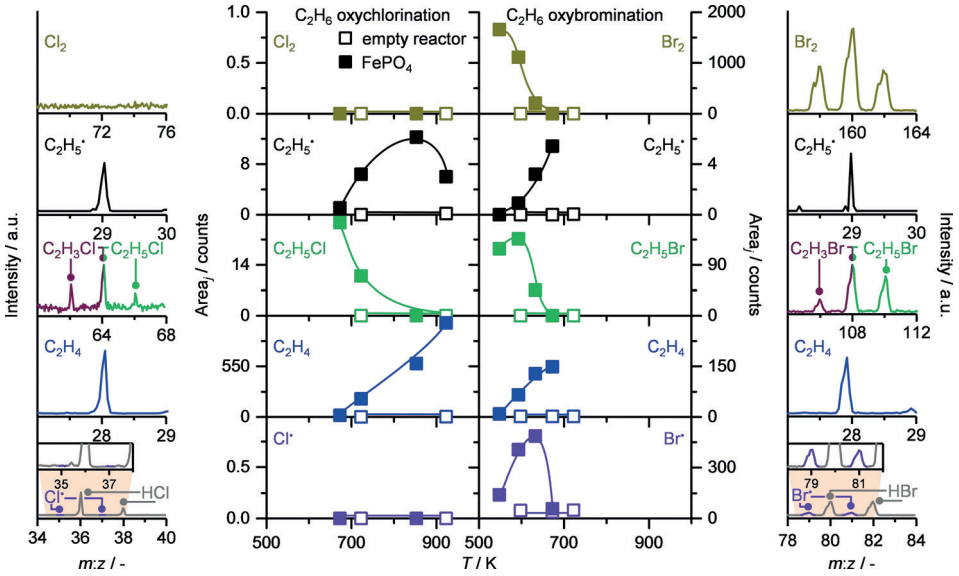

Figure 4. Extracted peak areas corresponding to molecular halogen, ethyl radical, ethyl halide, ethylene, and halogen radical as a function of temperature in the oxychlorination and oxybromination of ethane over $FePO_4$ and using an empty reactor as determined in operando PEPICO (middle panel). More details on the working principles of this technique are summarized in Scheme S2. The left and right panels illustrate the representative mass spectra of reactants, products, and intermediate radical species detected in ethane oxychlorination and oxybromination over $FePO_4$ at 723 K and 593 K, respectively. Conditions: C_2H_6:HX:O_2:Ar = 2:2:1:17, $F_T = 22\ cm^3\ min^{-1}$, $W_{cat} = 0.05$ or 0 g, $P = 2\times10^{-2}$ bar. The photon energies at which the signals of each chemical species were recorded in all PEPICO experiments are shown in Figures S6-S11.

gas-phase contributions are negligible, points to its role as an intermediate in the surface-confined mechanism, while its spectroscopic detection can be rationalized owing to its easy desorption from the catalyst (endothermic by 0.47 eV, Figure 5; Figures S5 and S14–S18), and the low reaction pressures (ca. 2×10^{-2} bar). In general, surface oxyhalogenation reactions require an Fe site with a neighboring oxygen and its halogenated counterpart (the latter are more prominent in oxychlorination, as determined by operando PGAA (Figure 3)), which are responsible for ethane activation and for ethyl halide dehydrohalogenation, respectively (Figure S14, Table S3). In particular, the former site allows for halogen-independent H stripping from ethane ($E_a = 0.61$ eV, Figure 5), which is however unlikely to catalyze H stripping from ethyl halide ($E_a > 2.10$ eV, Figure S14). Ethyl halide is formed through barrierless halogen addition to a surface-bound $C_2H_5^{\cdot}$ species (Figures S14–S18), which entails that only a small fraction evolves to the gas-phase provided a halogen atom is close. Further transformation of ethyl halide to ethylene requires a halogenated Fe site, where the halogen strips a hydrogen and generates the halide, thus closing the halogen cycle and highlighting the importance of surface halogen coverage for olefin formation. A chlorinated site favors this step by 0.18 eV over the brominated analogue (Figure S14)—in line with the observed 40 K light-off temperature shift in the dehydrohalogenation of ethyl halide (Figure S3). Furthermore, Cl stripping from the C_2H_4X intermediate to form C_2H_4 ($E_a = 0.67$ eV) is favored over Br stripping ($E_a = 1.50$ eV, Figure S14). However, considering the different extent of surface halogenation in oxychlorination and oxybromination (as determined by operando PGAA) and the possibility that a halogenated site enables concerted H and Cl abstraction from ethyl halide (Figure S14), which is favored over the individual steps by 0.29 eV, the most likely situation is that dehydrochlorination occurs in a concerted pathway on a chlorinated Fe site, while dehydrobromination occurs on an oxidic site in two individual steps (Figure 5; Figures S16–S18). Notably, in addition to the critical role that the halogen assumes in ethyl halide activation, it is even indirectly involved in ethane activation with oxygen, as evidenced by the complete absence of $C_2H_5^{\cdot}$ radicals in the PEPICO studies with halide-free feeds (Figures S7 and S9), and corroborated by the promoting effect of chlorine in oxidative dehydrogenation.[2a,9] This can be explained by the change of the oxidation state of iron upon

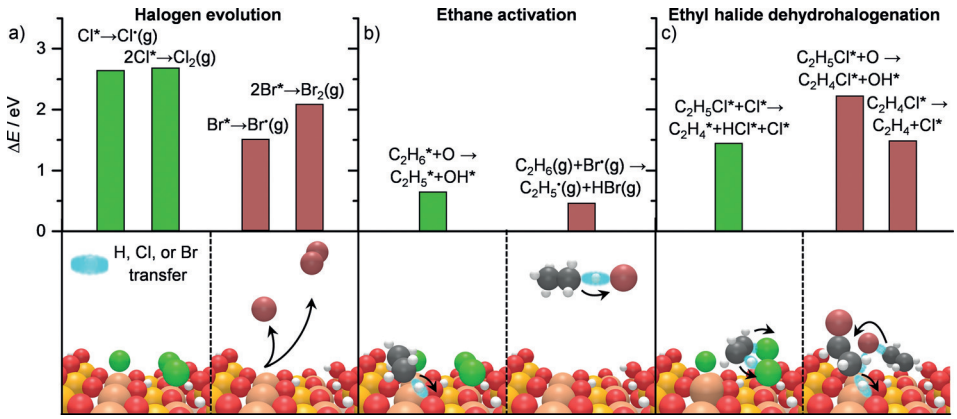

Figure 5. a) Energy barriers for halogen evolution, b) ethane activation, and c) ethyl halide dehydrohalogenation in ethane oxyhalogenation over a halogenated $FePO_4$(102) surface. The bottom panels illustrate the events corresponding to the respective bar plots that occur over the surface or in the gas-phase. Color code: Fe (light brown), P (yellow), O (red), Cl (green), Br (brown), C (gray), H (white). The complete reaction profile of the depicted most likely steps is provided in Figure S18.

halogen adsorption and the resulting structural rearrangement of the surface (Figure S19), as indicated by a Bader charge analysis (Table S4).[10] Thus, these changes of the electronic structure allow easier ethane activation when spectator halogen species are present—in contrast to a clean surface where the ethane activation has to overcome a 1.11 eV larger energy barrier.

In conclusion, we unraveled the mechanistic origin of the distinct selectivity patterns between ethane oxychlorination and oxybromination over iron phosphate by a multi-technique approach, which combined evidence from steady-state kinetics and operando PGAA and PEPICO spectroscopies, and was ultimately rationalized with theoretical calculations. The sharp selectivity control in oxychlorination is achieved by a purely surface-driven functionalization of ethane into ethyl chloride, which is further dehydrochlorinated to ethylene over a Cl–Fe center. In contrast, alkane activation to ethyl bromide in oxybromination occurs in the gas-phase with evolved bromine and bromine radical species, thus leaving a halogen-free surface that is more prone to additional cracking and combustion pathways. These results demonstrate that chlorine-based processes hold great potential for one-step olefin production in technical scale and provide guidelines for catalyst design for direct alkane-to-olefins transformation via oxyhalogenation. Furthermore, the findings provide a strategy for unraveling the mechanistic picture in a complex reaction network, which is the typical scenario encountered in virtually all hydrocarbon functionalization processes.

Acknowledgements

This work was supported by an ETH Research Grant ETH-04 16-1. P.H. and A.B. acknowledge funding by the SFOE (SI/501269-01). L.S. thanks the János Bolyai Research Fellowship of the Hungarian Academy of Sciences, as well as the Project No. 124068 of the National Research, Development and Innovation Fund of Hungary, financed under the K_17 funding scheme. We thank the Budapest Neutron Centre's transnational user access program for funding the PGAA beamtime. The authors thank Prof. Ralph Spolenak for access to Raman spectroscopy and Dr. Detre Teschner for providing accessories for the PGAA experiments. We thank Ali Saadun, Boglárka Maróti, and Ildikó Harsányi for assistance with the PGAA measurements, and Florian Goedicke for help with the PEPICO experiments.

Conflict of interest

The authors declare no conflict of interest.

[1] a) R. Lin, A. P. Amrute, J. Pérez-Ramírez, *Chem. Rev.* **2017**, *117*, 4182 – 4247; b) E. McFarland, *Science* **2012**, *338*, 340 – 342; c) H. Schwarz, *Angew. Chem. Int. Ed.* **2011**, *50*, 10096 – 10115; *Angew. Chem.* **2011**, *123*, 10276 – 10297; d) J. J. Sattler, J. Ruiz-Martinez, E. Santillan-Jimenez, B. M. Weckhuysen, *Chem. Rev.* **2014**, *114*, 10613 – 10653; e) J. F. Hartwig, *J. Am. Chem. Soc.* **2016**, *138*, 2 – 24; f) R. Horn, R. Schlögl, *Catal. Lett.* **2015**, *145*, 23 – 39; g) A. I. Olivos-Suarez, À. Szécsényi, E. J. M. Hensen, J. Ruiz-Martinez, E. A. Pidko, J. Gascon, *ACS Catal.* **2016**, *6*, 2965 – 2981.

[2] a) C. A. Gärtner, A. C. van Veen, J. A. Lercher, *ChemCatChem* **2013**, *5*, 3196 – 3217; b) F. Cavani, N. Ballarini, A. Cericola, *Catal. Today* **2007**, *127*, 113 – 131; c) K. Kwapien, J. Paier, J. Sauer, M. Geske, U. Zavyalova, R. Horn, P. Schwach, A. Trunschke, R. Schlögl, *Angew. Chem. Int. Ed.* **2014**, *53*, 8774 – 8778; *Angew. Chem.* **2014**, *126*, 8919 – 8923; d) C. A. Carrero, R. Schlögl, I. E. Wachs, R. Schomäcker, *ACS Catal.* **2014**, *4*, 3357 – 3380; e) V. Paunović, P. Hemberger, A. Bodi, N. López, J. Pérez-Ramírez, *Nat. Catal.* **2018**, *1*, 363 – 370.

[3] G. Zichittella, N. Aellen, V. Paunović, A. P. Amrute, J. Pérez-Ramírez, *Angew. Chem. Int. Ed.* **2017**, *56*, 13670 – 13674; *Angew. Chem.* **2017**, *129*, 13858 – 13862.

[4] a) V. Paunović, G. Zichittella, M. Moser, A. P. Amrute, J. Pérez-Ramírez, *Nat. Chem.* **2016**, *8*, 803 – 809; b) G. Zichittella, B. Puértolas, V. Paunović, T. Block, R. Pöttgen, J. Pérez-Ramírez, *Catal. Sci. Technol.* **2018**, *8*, 2231 – 2243; c) G. Zichittella, B. Puértolas, S. Siol, V. Paunović, S. Mitchell, J. Pérez-Ramírez, *ChemCatChem* **2018**, *10*, 1282 – 1290.

[5] U. Olsbye, O. V. Saure, N. B. Muddada, S. Bordiga, C. Lamberti, M. H. Nilsen, K. P. Lillerud, S. Svelle, *Catal. Today* **2011**, *171*, 211 – 220.

[6] G. L. Molnár, *Handbook of Prompt Gamma Activation Analysis with Neutron Beams*, Springer, Heidelberg, **2004**.

[7] Z. Révay, T. Belgya, L. Szentmiklósi, Z. Kis, A. Wootsch, D. Teschner, M. Swoboda, R. Schlögl, J. Borsodi, R. Zepernick, *Anal. Chem.* **2008**, *80*, 6066 – 6071.

[8] a) D. L. Osborn, C. C. Hayden, P. Hemberger, A. Bodi, K. Voronova, B. Sztaray, *J. Chem. Phys.* **2016**, *145*, 164202; b) X. Tang, G. A. Garcia, L. Nahon, *J. Phys. Chem. A* **2015**, *119*, 5942 – 5950; c) P. Osswald, P. Hemberger, T. Bierkandt, E. Akyildiz, M. Kohler, A. Bodi, T. Gerber, T. Kasper, *Rev. Sci. Instrum.* **2014**, *85*, 025101; d) P. Hemberger, V. B. F. Custodis, A. Bodi, T. Gerber, J. A. van Bokhoven, *Nat. Commun.* **2017**, *8*, 15946; e) P. Hemberger, A. J. Trevitt, T. Gerber, E. Ross, G. da Silva, *J. Phys. Chem. A* **2014**, *118*, 3593 – 3604.

[9] C. P. Kumar, S. Gaab, T. E. Müller, J. A. Lercher, *Top. Catal.* **2008**, *50*, 156 – 167.

[10] A. Walsh, A. A. Sokol, J. Buckeridge, D. O. Scanlon, C. R. A. Catlow, *Nat. Mater.* **2018**, *17*, 958 – 964.